HHS Public Access

Author manuscript

Neuron. Author manuscript; available in PMC 2019 September 19.

Published in final edited form as:

Neuron. 2018 September 19; 99(6): 1289–1301.e2. doi:10.1016/j.neuron.2018.08.008.

CORRELATION OF SYNAPTIC INPUTS IN THE VISUAL CORTEX OF AWAKE BEHAVING MICE

Sergio Arroyo[#1,2], **Corbett Bennett**[#1,3], and **Shaul Hestrin**[1,4,†]

[1]Department of Comparative Medicine, Stanford University School of Medicine, Stanford, CA 94305, USA.

[2]Current address: Massachusetts General Hospital, Department of Neurology, Harvard Medical School, Boston, MA 02114, USA

[3]Current address: Allen Institute for Brain Science, Seattle, WA 98109, USA.

[4]Lead contact

[#] These authors contributed equally to this work.

Summary

The subthreshold mechanisms that underlie neuronal correlations in awake animals are poorly understood. Here, we perform dual whole-cell recordings in the visual cortex (V1) of awake mice to investigate membrane potential (Vm) correlations between upper layer sensory neurons. We find that the membrane potentials of neighboring neurons display large, correlated fluctuations during quiet wakefulness, including pairs of cells with disparate tuning properties. These fluctuations are driven by correlated barrages of excitation followed closely by inhibition (~5 ms lag). During visual stimulation, low-frequency activity is diminished, and coherent high-frequency oscillations appear, even for non-preferred stimuli. These oscillations are generated by alternating excitatory and inhibitory inputs at a similar lag. The temporal sequence of depolarization for pairs of neurons is conserved during both spontaneous and visually-evoked activity, suggesting a stereotyped flow of activation that may function to produce temporally precise “windows of opportunity” for additional synaptic inputs.

eTOC

Arroyo et al. examine the correlation of subthreshold synaptic activity in superficial neurons of primary visual cortex in awake mice, providing new insights into the function of neuronal correlations and the mechanisms that generate them.

[†]To whom correspondence should be addressed: shestrin@stanford.edu.

Author Contributions

Conceptualization: S.A., C.C.B., and S.H.; Software: S.A., C.C.B., and S.H.; Investigation: S.A., C.C.B.; Writing (original draft, review and editing): S.A., C.C.B., and S.H.; Visualization: S.A., C.C.B.; Resources: S.H.; Supervision: S.H.

Declaration of Interests

None

Introduction

Correlations in the spiking of sensory neurons are thought to have a profound impact on their ability to encode and transmit information. While pairwise spiking correlations are known to depend on sensory stimulation and behavioral state (Averbeck et al., 2006; Cohen and Kohn, 2011; Ecker et al., 2010; Fries, 2005; Gregoriou et al., 2009), the mechanisms underlying these correlations are unclear, in part because previous studies have relied on extracellular recording techniques that cannot probe the synaptic inputs underlying correlated activity(Cohen and Kohn, 2011; Doiron et al., 2016). In theory, changes in spike correlation could reflect changes in excitatory, inhibitory, and/or modulatory inputs (Doiron et al., 2016; McGinley et al., 2015b). Intracellular recordings in the awake animal can provide information on the dynamics of shared changes in excitability across behavioral states, and the synaptic components which drive them (Okun and Lampl, 2008).

Several studies have demonstrated large-amplitude, slow Vm fluctuations during sleep, similar to the so-called “up/down” fluctuations reported in the anesthetized animal (Cohen-Kashi Malina et al., 2016; Cowan and Wilson, 1994; Lampl et al., 1999; Lemieux et al., 2015; Okun and Lampl, 2008; Sheroziya and Timofeev, 2014; Steriade et al., 1993; Wilson and Groves, 1981; Yu and Ferster, 2010). Originally it was suggested that these large, correlated Vm fluctuations were abolished during wakefulness, when cortex entered an asynchronous state characterized by a depolarized Vm (Steriade et al., 2001).

Surprisingly, however, whole-cell recordings in somatosensory cortex of un-anesthetized mice revealed that a synchronized state generally resembling slow wave sleep and anesthesia is also exhibited during quiet wakefulness (Crochet and Petersen, 2006). Subsequent intracellular recordings in rodents and primates have extended these findings to visual, auditory and motor cortices, demonstrating that large-amplitude, low frequency Vm fluctuations are a hallmark of cortical activity during quiet wakefulness. Interestingly, these dynamics are rapidly suppressed by arousal associated with either motor activity or pupil dilation (Bennett et al., 2013; Einstein et al., 2017; McGinley et al., 2015a; Polack et al., 2013; Reimer et al., 2014; Schiemann et al., 2015; Schneider et al., 2014).

Are Vm fluctuations during quiet wakefulness correlated across neighboring neurons? In somatosensory cortex, correlated slow (1–10 Hz) Vm fluctuations have been recorded in excitatory and inhibitory neurons during quiet wakefulness that are suppressed during whisking or movement (Gentet et al., 2010; Gentet et al., 2012; Poulet and Petersen, 2008; Zhao et al., 2016). However, these studies used transient stimuli to probe sensory responses and therefore could not investigate how subthreshold correlations are modulated during persistent sensory stimulation.

In visual cortex, dual intracellular recordings in anesthetized animals demonstrated that the membrane potential of neighboring neurons is highly correlated in the absence of visual stimulation ($r > 0.5$) (Lampl et al., 1999; Yu and Ferster, 2010), but that sensory stimulation largely suppresses low frequency correlations and enhances Vm correlations in a high frequency band (Lampl et al., 1999; Yu and Ferster, 2010). However, anesthesia has been shown to dramatically suppress inhibition and neuronal excitability (Haider et al., 2013), and

precludes the interrogation of the impact of behavioral state. In awake macaque V1 it was shown that visual stimulation reduced slow membrane potential fluctuations and Vm/LFP coupling, but the effect on subthreshold Vm correlations between cells was not explored (Tan et al., 2014).

To investigate how visual stimulation and behavioral states affect membrane potential correlation we have performed simultaneous WC/LFP, LFP/LFP, and WC/WC recordings from the superficial layers of visual cortex in awake mice allowed to move or remain stationary on a spherical treadmill. We found that the membrane potential of L2/3 neurons in visual cortex was highly correlated over large distances and independent of preferred orientation. Visual stimulation reduced low frequency (3–10 Hz) correlations and generated correlated high frequency (20–50 Hz) oscillations. Furthermore, correlation analysis indicated that pairs of L2/3 neurons maintained consistent lead/lag during both spontaneous activity and visual stimulation. By obtaining dual current clamp/voltage clamp recordings, we investigated the excitatory and inhibitory synaptic mechanisms that underlie correlations in Vm. We found that Vm fluctuations are generated by an increase in excitation followed by an increase in inhibition. Finally, we demonstrated that fast synaptic inputs leading to action potentials were shared between pairs of cells during visual stimulation but not spontaneous activity.

Results

The spatial extent of correlated neuronal activity in the visual cortex of awake, behaving mice

The local field potential (LFP) is thought to represent the averaged activity of many neighboring neurons (Haider et al., 2016; Katzner et al., 2009). To investigate the extent to which the subthreshold membrane potential fluctuations in individual L2/3 pyramidal neurons are correlated with neighboring cells, we obtained simultaneous WC/LFP recordings during presentation of a uniform gray screen (Figure 1A). The mice were allowed to move or remain stationary on a spherical treadmill, as described previously (Dombeck et al., 2007). Under these conditions, we found a high level of correlation between Vm and the simultaneously recorded LFP (1–100 Hz) during quiet wakefulness (Figure 1B upper; Figure 1C, D, black traces; Supplemental Table 1) that was reduced during locomotion (Figure 1B lower; Figure 1C, D, red traces; Supplemental Table 1). These data suggest that the subthreshold activity in single cells is reflected in the averaged population activity of many neighboring neurons (Haider et al., 2016; Okun et al., 2010).

We next investigated the extent to which the fluctuations present in both WC and LFP recordings during quiet wakefulness were correlated as a function of distance. To accomplish this, we performed dual LFP recordings across a span of ~1.2 mm (Figure 1E). In addition to physical distance, we also measured the retinotopic distance between the two LFP recordings (see Methods; Figure 1F). The receptive fields of the recording sites moved laterally and dropped in elevation as the craniotomies moved medially on the surface of the brain, as described previously (Wang and Burkhalter, 2007). These paired LFP recordings revealed a high level of correlation that was reduced with distance (Figure 1G; space constant of ~50 deg/500 microns). These data indicate that the low frequency, high

amplitude fluctuations in Vm and LFP during quiet wakefulness are correlated across a wide swath of primary visual cortex.

Spontaneous membrane potential correlations are independent of stimulus preference

In barrel cortex, the Vm of neighboring pyramidal cells in L2/3 respond to the same whisker and are highly correlated during quiet wakefulness (Poulet and Petersen, 2008). However, the Vm correlation of L2/3 cells in mouse V1, where neighboring neurons exhibit heterogeneous response properties, has not been studied. To determine the Vm correlation in primary visual cortex, we performed dual WC recordings from nearby cells (Figure 2A) in L2/3 of V1 in mice viewing a uniform gray screen. We observed that the large fluctuations observed during quiet wakefulness were highly correlated between pairs of neurons (Figure 2C), whereas the low-amplitude, high frequency activity during locomotion appeared less correlated (Figure 2B). To quantify this, we computed the cross-correlogram of the two signals. This analysis revealed high correlation during quiet wakefulness (Figure 2D, black trace, for pair shown in A; Figure 2F, black trace, for population average; Supplemental Table 1) that was reduced during locomotion (Figure 2D, red, for cell in A; Figure 2F, red, for population average). To determine whether these state-dependent correlations were driven by the low-frequency fluctuations observed during quiet wakefulness, we re-computed the cross-correlogram after high-pass filtering the signals (>20 Hz; Figure 2E for pair in A; Figure; 2G for population average). High frequency correlations were lower (Supplemental Table 1) and not sensitive to behavioral state, indicating that the state-dependent correlation in Figure 2F was primarily the result of the low-frequency, high-amplitude fluctuations during quiet wakefulness.

Which synaptic inputs contribute to correlated subthreshold activity? Previous studies have demonstrated that pyramidal neurons sharing similar stimulus preferences are highly interconnected (Ko et al., 2013; Ko et al., 2011). Thus, functionally similar neurons might be expected to exhibit higher levels of correlation due to their overlap in presynaptic partners. To test this possibility, we presented drifting gratings and calculated the preferred orientation disparity between each pair of neurons. We then plotted both the raw Pearson's r and the high-passed filtered (>20 Hz) Pearson's r as a function of this tuning difference (Figure 2I). We found that neither the high-passed filtered nor the unfiltered correlation was dependent on the similarity in stimulus preferences. These data suggest that the high levels of correlation across L2/3 pyramidal cells are not generated by the synaptic connections between functionally related neurons in L2/3.

The lag between slow Vm fluctuations in pairs of L2/3 neurons is consistent

The large Vm fluctuations that drive L2/3 correlations could propagate randomly through the local network. Alternatively, these depolarizing waves could travel through stereotyped pathways that preserve a temporal order of activation. Consistent with the latter possibility, we observed that the peak in the averaged cross-correlogram was offset from zero in several pairs, suggesting that some cells may lead others during shared membrane potential fluctuations (Figure 3A, B). To further explore this relationship, we calculated the cross correlogram (CCG) for individual trials and plotted the lag between the cells over time (see Methods). This analysis revealed that the sign of the offset was consistent from trial to trial,

indicating a conserved order of activation for pairs of cells (Figure 3C). This offset in the peak of the CCG was significant for 6/10 pairs (Figure 3D). Lags for cells during stationary epochs were correlated with lags observed during moving epochs (Supplemental Figure 1).

The role of excitation and inhibition in generating spontaneous Vm correlations during quiet wakefulness and locomotion

The spontaneous correlated fluctuations in Vm during quiet wakefulness could result from underlying changes in the relative timing or amplitude of excitation and/or inhibition. To understand how inhibitory and excitatory inputs converge to produce correlated Vm fluctuations, we first obtained a current clamp recording to monitor membrane potential fluctuations. Because these fluctuations are highly correlated across neighboring cells (Figure 2), we used this current clamp recording as a reference for the state of the local network. We then obtained a simultaneous voltage clamp recording from a nearby cell (< 200 microns) to determine the temporal relationship between excitation/inhibition and the shared network fluctuations.

First, we examined the changes in excitation and inhibition that accompanied the depolarized, or “up,” and hyperpolarized, or “down,” phases of fluctuations (see Methods). During quiet wakefulness, large depolarizations were correlated with concomitant increases in excitation (Figure 4A, left) and inhibition (Figure 4A, right). Indeed, when we averaged the mean excitatory and inhibitory currents during “up” phases and compared these currents to those measured during “down” phases, we found a significant increase in both excitation and inhibition during the “up” phase (Figure 4B, Supplemental Table 2). Similar to Vm-Vm correlations, we found that Vm/excitation correlation did not depend on turning similarity (Supplemental Figure 3B).

To compute the lag between excitatory and inhibitory conductances, we computed the CCGs for excitation-Vm and inhibition-Vm, using the current clamp recording as a temporal reference. We then compared the offsets in the peaks of these mean CCG waveforms (Figure 4C). We also calculated the median offset between CCGs calculated for individual trials (Figure 4D). Both of these analyses revealed that inhibition lagged excitation by ~ 5 milliseconds (mean CCG offset 3 ms ± 1.1, n=8; median CCG offset 4.9 ± 1.1 ms, n=8).

We also analyzed the lag between excitation and inhibition by manually identifying transitions to the “up” and “down” phases of the fluctuations. Over our population of cells, we found that excitation led inhibition on transitions to the “up” phase (Supplemental Figure 2A, left). In contrast, we did not observe significant latency between excitation and inhibition for transitions to the “down,” suggesting that this transition reflects a gradual dwindling of synaptic inputs and not an active process that is initiated by an increase in inhibition (Supplemental Figure 2A, right; Supplemental Figure 2B).

During locomotion, the large, coordinated changes in excitation and inhibition that accompanied Vm fluctuations were suppressed (Figure 4E) and the variance in both excitatory and inhibitory inputs was reduced (p=0.03 and 0.02, respectively; Figure 4F). Thus, the Vm decorrelation we observe during locomotion likely reflects reduced synchronization of both excitatory and inhibitory synaptic inputs.

Visual stimulation diminishes low-frequency and enhances high-frequency correlations

How does sensory stimulation affect correlations between neurons in visual cortex? To address this question, we examined subthreshold Vm correlations between V1 neurons during the presentation of drifting sinusoidal gratings (Figure 5A). During quiet wakefulness, visual stimulation reduced overall Vm correlations (Figure 5B, C) but introduced high-frequency, synchronous oscillations (Figure 5D). Similar to spontaneous Vm correlations, correlations during the visual stimulus did not depend on tuning similarity (Supplemental Figure 3A). To estimate the average amplitude of the visually evoked oscillations we detected large events (> 2.75 mV) in band-filtered (20–80 Hz) traces. We then used the detected events to align and average segments of traces recorded in the two cells (Figure 5D, inset). We found that the ratio of the event amplitude in the paired cell to the event amplitude in the trigger cell was significantly larger than shuffled data (ratio = 0.39 ± 0.05 vs. ratio = 0.05 ± 0.001; P = 0.0078, n = 8 pairs; Wilcoxon signed rank 2-tail test).

We compared the coherence of the membrane potentials of the two cells during visual stimulation to the coherence during presentation of a gray screen (Figure 5E). This analysis (averaged across 10 pairs) revealed both a significant decrease in coherence at low frequencies (1–10Hz) and an increase in coherence at high frequencies (15–40 Hz) (n=10; Figure 5F; Supplemental Table 1). In individual cells, power in this band (15–40 Hz) was significantly less tuned for orientation than spiking (spiking OSI: 0.63 +/− 0.05, high frequency power OSI: 0.17 +/− 0.02, p = 9e-5). High frequency coherence between cells in a pair was not tuned for orientation (OSI= 0.05 +/− 0.01).

We next asked how visual stimulation affected the temporal relationship between pairs of cells. Despite reducing the coherence between cells at low frequencies, we often observed that slow, correlated Vm fluctuations persisted during visually-evoked activity (Supplemental Figure 4A). These fluctuations did not reflect F1 modulation as they were not time-locked to the stimulus. To analyze the timing between cells for both fast and slow Vm fluctuations, we first filtered the signals (1) with a high-pass filter above 3 Hz to remove F1 stimulus-evoked modulations but preserve low-frequency (< 10 Hz) fluctuations and (2) a band pass filter (15–50 Hz) to a capture the high frequency activity elicited by visual stimulation. We then analyzed the CCG offset as described in Figure 2 using these two filtered signals. Interestingly, we found that the lag between cells during visually-evoked activity was significantly correlated with the lag during spontaneous activity when both were filtered at > 3 Hz (Supplemental Figure 4B). In turn, the lag between cells during spontaneous activity, when filtered to capture high frequency activity (15–50 Hz), was also highly correlated with the lag computed using the > 3 Hz filter (Supplemental Figure 4C). Moreover, neither the lag during spontaneous activity nor during visual stimulation was sensitive to behavioral state (Supplemental Figure 1). Thus, while visual stimulation alters the spectral pattern of correlations by enhancing high-frequency and diminishing low-frequency fluctuations, the temporal relationship between pairs of neurons at both high and low frequencies is preserved and correlated with the temporal lag observed during quiet wakefulness.

Trial-to-trial variability in the correlation and frequency of visually evoked Vm fluctuations

The above data suggest that, on average, the fast Vm fluctuations during visual stimulation are highly correlated between cells. However, even within the same behavioral state of quiet wakefulness, we often noticed wide variability in the amplitude and frequency of these visually-evoked fluctuations. To illustrate this, we computed the trial-to-trial Pearson's correlation on filtered Vm (15–50 Hz) for one pair of neurons during presentation of visual gratings while the animal remained stationary (Figure 5G, left). Under these conditions, the filtered Vm correlation varied widely between ~0.3 and ~0.7; CCGs illustrating the two extremes of this spectrum are depicted to the right (Figure 5G, right). Furthermore, we also noted trial-to-trial variability in the frequency of these fluctuations. To visualize the frequency components of Vm waveforms during visual stimulation, we computed spectrograms for each cell for individual trials. We noticed a striking variability in the power between 15–50 Hz in these spectrograms, with some trials exhibiting predominant power in the lower beta frequency range (Figure 5H, top) while others showed peaks at higher frequencies (Figure 5H, bottom), despite the fact that all trials were taken from the same behavioral state and stimulus contrast. To quantify this we calculated the frequency center of mass (COM) for each pair of recorded neurons from trial to trial. This analysis revealed that the COM for visually evoked fluctuations was variable and correlated with the COM of the simultaneously recorded neuron (Figure 5I). Together, these data demonstrate that the amplitude and the frequency of visually-evoked oscillations are dynamic and correlated across L2/3 cells.

Inhibition lags excitation during visually-evoked Vm oscillations

What synaptic conductances drive the high-frequency oscillations induced by visual stimulation? To address this question, we analyzed paired current-clamp/voltage-clamp recordings during the presentation of drifting gratings. We observed rhythmic excitatory (Figure 6A, B) and inhibitory (Figure 6C, D) post-synaptic currents that were phase-locked to the Vm oscillations measured in the paired current-clamp recording (Figure 6B,D). Indeed, both excitatory and inhibitory inputs exhibited a dramatic increase in coherence with Vm in the 15–40 Hz frequency band during visual stimulation (Figure 6E; Supplemental Table 2), consistent with our paired current-clamp recordings (Figure 5F; Supplemental Table 1).

We next examined the relative timing of excitatory and inhibitory currents during these high frequency oscillations. For each VC/CC pair, we first bandpass-filtered the signals at 15–40 Hz to isolate visually evoked oscillations. We then computed the CCG for excitation-Vm and inhibition-Vm. By comparing the offsets in the peaks for these CCGs, we were able to determine the relative timing of excitatory and inhibitory inputs. This analysis revealed that inhibition significantly lagged excitation by ~4 ms (Figure 6F,G; Supplemental Table 2).

Visual stimulation is followed by large, highly correlated Vm fluctuations

During quiet wakefulness, we often observed a bout of several high-amplitude Vm fluctuations following visual stimulation (10/13 pairs; Figure 7A, upper; Supplemental Figure 5) lasting for several hundred milliseconds. These fluctuations were reduced during moving (Figure 7A, lower). The magnitude of these fluctuations varied from trial to trial but

was highly correlated between simultaneously recorded neurons (Figure 7B), suggesting that these fluctuations reflected shared synaptic inputs. Moreover, when quantified as the power in the 2–10 Hz frequency band, these post-stimulus fluctuations were significantly more prominent than those observed during quiet wakefulness (Figure 7C). Locomotion increased spike probability during visual stimulation (Bennett et al., 2013; Niell and Stryker, 2010; Polack et al., 2013) but suppressed spike probability during the post-stimulation period (Fig. 7D). Interestingly, we observed an increased spike rate during the crests of the post-stimulus period that was significantly greater than the baseline spontaneous firing rate and comparable to the peak firing rate during visual stimulation (Figure 7D).

To investigate the synaptic mechanisms underlying these post-stimulation fluctuations, we recorded from one neuron under current clamp while simultaneously recording a second neuron under voltage clamp held at the reversal potential for excitation (Figure 7E, left) or inhibition (Figure 7E, right). We found that immediately following visual stimulation there was a short ~50 ms window of hyperpolarization which corresponded to a decrease in both excitatory and inhibitory inputs (Figure 7E, inset). Following this epoch, Vm depolarizations corresponded to large barrages of both excitation and inhibition, similar to the pattern of conductances underlying spontaneous Vm fluctuations during quiet wakefulness.

We then asked whether the temporal relationship between cells during this pattern activity was preserved when compared to other conditions. As described previously, we calculated the cross correlogram between the Vm of simultaneously recorded cells, and computed the CCG offset to determine the temporal lag between them (Figure 7F, G). We found that the CCG offset between pairs during post-stimulation was correlated with the CCG offset during spontaneous activity, though this correlation did not reach significance ($p = 0.06$). Overall, the level of Vm correlation observed during the post-stimulus epoch during both quiet wakefulness and locomotion exceeded those observed with or without visual stimulation (Figure 7H).

Synaptic inputs leading to action potentials are more coordinated across cells during visual stimulation

The membrane potential correlations we have described may provide windows of opportunity for coordinated spiking in neighboring cells. The precision of this synchrony depends on the temporal relationship of the synaptic inputs that are associated with action potentials across cells.

To address whether Vm correlations occur within narrow temporal windows surrounding the generation of action potentials, we computed the spike triggered average (STA) of the membrane potential for both the spiking cell and the simultaneously recorded cell in each pair. This method allowed us to compare the patterns of inputs that drive spontaneous and visually-evoked spiking activity (by examining the spiking cell STA), and to measure the temporal relationship of inputs in neighboring cells (by examining the paired cell STA).

Analysis of the pre-spike depolarization (PSD) revealed that the majority of excitation preceding spikes was not shared across cells (Figure 8A and B, Supplemental Figure 6A and B), similar to what has been reported in barrel cortex (Poulet and Petersen, 2008). The

paired PSD was significantly attenuated during movement and visual stimulation relative to stationary epochs, likely reflecting the suppression of correlated membrane potential fluctuations (Figures 2 and 5, respectively).

To better examine the inputs that immediately precede action potentials, we band-pass filtered the STAs for each pair in the 15–40 Hz range. Filtering in this band removed slow covariation and revealed high frequency activity on the time scale of synaptic inputs. Filtered STAs showed that a small depolarization prior to spiking was shared in the paired cell (trough-to-peak amplitude of ~0.4 mV) during visually-evoked but not spontaneous activity (Figure 8C), consistent with the increase in coherence seen at high frequencies during visual stimulation (Figure 5). Plotting the size of the shared depolarization against the disparity in orientation preference for the cells in each pair revealed no dependence of the PSD on tuning similarity at fast or slow timescales (Supplemental Figure 6C and D).

Discussion

We investigated neuronal correlations of layer 2/3 neurons in primary visual cortex of awake mice using dual whole-cell recordings. We find that the membrane potentials of cortical cells in L2/3 are highly correlated, including cells with disparate tuning preferences, largely due to slow Vm fluctuations that are detectable in the LFP for up to 0.5 mm. Both locomotion and visual stimulation diminished spontaneous, low-frequency Vm correlations. Large, correlated fluctuations in Vm during quiet wakefulness are mediated by increases in synaptic excitation followed by inhibition (lag of ~5 ms). Visual stimulation generates high-frequency (20–50 Hz), large amplitude (5–10 mV) correlated membrane potential oscillations. These visually-evoked high frequency oscillations are driven by excitatory inputs followed by inhibition with a delay ~5 ms. Visual stimulation is followed by highly correlated ~4 Hz oscillations lasting about 1 second. Across all conditions we examined, the pairwise temporal relationship between neurons is preserved, suggesting a conserved pattern of activation in cortical networks. Finally, we showed that during visual stimulation fast synaptic inputs leading to action potentials were partially shared between pairs of cells. Together, these data provide new insights into the function of Vm correlations in cortical networks of the awake, behaving animal, as well as the mechanisms that generate them.

Functional implications for layer 2/3 network structure

Previous studies have demonstrated that L2/3 neurons in visual cortex form interconnected subnetworks defined by their tuning preferences and subfield overlap (Hofer et al., 2011; Ko et al., 2013; Ko et al., 2011). We found that slow Vm correlations are independent of stimulus preference. These data suggest that L2/3 Vm fluctuations are driven primarily by external, correlated synaptic inputs rather than local inputs from functionally related neighboring cells. This network property is further supported by the fact that we found a high level of correlation between Vm and LFP. Moreover, we show that the LFP is highly correlated across visual cortex with a space constant of ~500 microns, suggesting Vm correlations extend across more than 50 degrees of visual space. Note, however, that the passive spread of the LFP signal may increase the measured correlation between electrodes; nonetheless, the value we report may be considered an upper bound on the true correlation

driven by local neuronal activity. These findings are consistent with the principle that Vm correlations are governed primarily by anatomical distance rather than response preference. It was reported that in anesthetized cat pairwise correlations of Vm in L2/3 neurons can be related to orientation preferences (Yu and Ferster, 2010). The difference between our findings and those of Yu and Ferster may be related to anesthesia or cortical organization. For example, in the mouse visual cortex cells of disparate tuning properties are interspersed, whereas in the cat nearby cells likely belong to the same orientation column, confounding the effects of distance and tuning similarity on correlation.

Cortical slow waves (a.k.a. up/down states) have been previously observed during non-REM sleep (Steriade et al., 2001; Timofeev et al., 2001). It was suggested that the depolarized phase (i.e., up state) of these waves can synchronize activity between cortical and hippocampal circuits and drive synaptic plasticity during memory consolidation (Rothschild et al., 2017; Siapas and Wilson, 1998; Sirota et al., 2003). However, the role of the slow fluctuations in the awake state is not known. We propose that strong correlation of cells, independent of their properties, within V1 and perhaps across other brain areas, would allow efficient processing of spikes generated during the up state. In contrast, sensory stimulation and other external inputs that are not phase locked to the internal fluctuations may arrive during the down state and will be suppressed (Bennett et al., 2013; Einstein et al., 2017). Therefore, the correlated fluctuations may be a mechanism to distinguish inputs generated by the local network from inputs originating from sensory organs or distal brain areas that are not phase locked to the slow fluctuations.

Previous studies, using extracellular recordings or imaging, have demonstrated that ensembles of cortical cells can spike in predictable sequences that are preserved across stimulation protocols and behavioral states (Euston et al., 2007; Harvey et al., 2012; Jermakowicz et al., 2009; Ji and Wilson, 2007; Luczak et al., 2007). It was proposed that temporally precise sequences of cortical activity underlie communication across cortical areas (Abeles, 1991) and are important for short term (Harvey et al., 2012) or long term memory (Euston et al., 2007; Ji and Wilson, 2007). However, the mechanisms that can generate consistent sequences of activation in the cortex are not understood. In theory, sequential spiking could be generated by temporally patterned synaptic inputs, whereby cells firing early in a sequence receive inputs prior to cells that fire late. Conversely, sequential spiking could reflect differences in excitability, whereby all cells receive coincident synaptic input and spike timing is determined by the time needed to reach threshold. Here we show that upper layer cortical cells receive a pattern of sequential synaptic inputs that is conserved across behavioral states and visual stimuli. These data suggest that synaptic activity flows through the cortical network in a stereotyped fashion, and may form the basis for sequential cortical computations.

Finally, we show that excitation and inhibition are tightly coupled in the awake cortex during both spontaneous and visually-evoked activity, with excitation leading inhibition by ~5 ms. Previous in vitro studies showed tight synchronization and correlation of excitation and inhibition (Salkoff et al., 2015). Moreover, studies in anesthetized animals found similar E-I coupling (Haider et al., 2013; Haider et al., 2016; Okun and Lampl, 2008), but the network effects of anesthesia (Haider et al., 2013) have called into question whether these results can

be generalized to the awake state. However, how excitation and inhibition interact to produce the synchronous, high-frequency oscillations frequently observed during visual stimulation has remained unclear. Here we demonstrate that both the slow fluctuations during spontaneous activity and the high frequency oscillations during visual stimulation are initiated by an excitatory barrage followed rapidly by inhibition. Our data thus suggest that stimulus-induced high frequency (beta and gamma) oscillations are generated by the interplay of excitatory and inhibitory networks, similar to the E-I model previously proposed (Buzsaki and Wang, 2012). We found that although the amplitude of the synchronous high-frequency oscillations was several mV (Figure 6), they rarely generated action potentials. These data suggest that additional depolarizing inputs are required to convert visually-evoked Vm synchrony to spike synchrony.

Circuit mechanisms underlying Vm correlations

In theory, eye movements could cause a coordinated signal across visual cortex, contributing to what we observe as spontaneous Vm correlations. However, we think this is unlikely for several reasons. First, spontaneous correlations were highest during quiet wakefulness, when mice rarely saccade (Bennett et al., 2013; Niell and Stryker, 2010). Second, mice saccade at a rate of less than 1 Hz, while the spontaneous correlated fluctuations we observed are shifted towards higher frequencies (~ 2–4 Hz). Finally, spontaneous correlations were measured during presentation of an isoluminant gray screen, for which saccades would not generate visual flow.

The insensitivity of Vm correlations during quiet wakefulness to stimulus preference suggest that some external input may drive many local sub-networks in parallel during transitions to “up” phases. Thalamic inputs could provide this drive; however, studies in the anesthetized cat and awake mouse suggest that slow, correlated cortical fluctuations persist in the absence of thalamic input (Timofeev et al., 2000). Others have demonstrated that silencing of layer 5 pyramidal neurons terminates the slow fluctuations seen in L2/3 during anesthesia (Beltramo et al., 2013), suggesting a cortical origin for shared Vm fluctuations. However, given that anesthesia has been shown to alter the cortical network (Adesnik et al., 2012; Haider et al., 2013), whether the mechanisms that generate up/down states during anesthesia underlie the slow fluctuations observed during quiet wakefulness needs further investigation.

Recent studies in several cortical areas have shown that locomotion is accompanied by a state transition in individual cells from slow, large-amplitude Vm fluctuations to a depolarized Vm with low variance (Bennett et al., 2013; Einstein et al., 2017; McGinley et al., 2015a; Polack et al., 2013; Reimer et al., 2014; Schiemann et al., 2015; Schneider et al., 2014). Here we show that this state transition decorrelates the membrane potential of neighboring cells. What mechanisms underlie this decorrelation? In the auditory cortex, projections from motor cortex have been shown to mediate the state transition at locomotion onset (Schneider et al., 2014). Similarly, in the barrel cortex, optogenetic activation of feedback projections from whisker motor cortex can reduce low-frequency activity (Zagha et al., 2013). However, it is unclear whether a similar mechanism underlies the locomotion-associated decorrelation we observe. Both noradrenergic and cholinergic fibers in V1 are activated during locomotion (Polack et al., 2013; Reimer et al., 2016), either of which could

mediate a reduction in Vm correlation. Indeed, activation of cholinergic pathways has been shown to reduce low frequency LFP power (Goard and Dan, 2009), and noradrenaline is necessary for the transition from synchronous to asynchronous dynamics during recovery from anesthesia (Constantinople and Bruno, 2011). Further work is needed to understand how these pathways converge to produce state transitions in V1.

During presentation of a prolonged visual stimulus of high contrast sinusoidal gratings, we observe the emergence of high frequency Vm oscillations in the 20–50 Hz frequency range. Similar visually-evoked ~30 Hz oscillations were previously demonstrated using paired intracellular recording in anesthetized cat and Vm-LFP recordings in V1 of awake mouse (Veit et al., 2017; Yu and Ferster, 2010). Modeling work has suggested that the frequency of Vm oscillations may be modulated by the delay between excitatory and inhibitory networks (Buzsaki and Wang, 2012; Tiesinga and Sejnowski, 2009). Interestingly, our voltage clamp recordings reveal concordant excitatory and inhibitory oscillations that accompany the fast visually-evoked Vm fluctuations, with inhibition lagging excitation by a similar lag (~5 ms) to the much slower oscillations observed during quiet wakefulness. Voltage clamp measurements of distal synaptic currents are significantly attenuated and slowed. Thus, somatic and proximal inhibitory inputs, originating mostly from PV-expressing neurons, would be less affected by voltage-clamp errors relative to excitatory inputs onto the distal dendritic arbor. As a result, under our experimental conditions, it is likely that the true lag of inhibition relative to excitation is larger than the one we measured. Moreover, distal inhibitory input from interneurons that target dendrites may be out of phase with somatic inhibition, as has been described in the barrel cortex (Gentet et al., 2012).

We show that fast Vm oscillations are highly correlated between pairs of neurons, suggesting that they reflect a global network phenomenon and may contribute to synchronized spiking. Indeed, we demonstrate that spike triggered average of Vm in the paired cell reveals a sharp depolarizing transient. Although these fast oscillations are typically of significant amplitude (5–10 mV), they remain below threshold and do not lead directly to the generation of action potentials. However, they may function to produce temporally precise “windows of opportunity” for additional synaptic inputs.

Following presentation of visual stimuli during quiet wakefulness, we show that L2/3 neurons exhibit a profound hyperpolarization, mediated by a reduction in both excitation and inhibition, followed by several low-frequency, high amplitude Vm fluctuations. These fluctuations were similar in appearance to the spontaneous fluctuations observed during quiet wakefulness, but were more rhythmic, more highly correlated, and drove spiking activity above baseline (Figure 7D). Similar visually-evoked fluctuations were recently reported in visual cortical neurons of awake behaving mice (Einstein et al., 2017). However, unlike Einstein et al., the post-stimulation fluctuations we observed occurred rarely during locomotion and, when they did occur, were significantly diminished in amplitude.

Comparison with previous studies

Several studies have shown that neighboring cortical neurons exhibit a high degree of membrane potential correlation in the anesthetized state (Lampl et al., 1999; Petersen et al., 2003; Volgushev et al., 2006). Under these conditions, large coordinated Vm depolarizations

or “up” states were shown to be driven by an increase in excitatory conductance followed by a concomitant increase in inhibitory conductance (Haider et al., 2006; Okun and Lampl, 2008). Similarly, we find that Vm fluctuations in the awake animal during quiet wakefulness are generated by an increase in both excitatory and inhibitory inputs, with inhibition lagging excitation by roughly 5 milliseconds.

To date, the only studies investigating Vm correlations between cortical neurons in the awake animal have been carried out in the somatosensory cortex (Poulet and Petersen, 2008; Zhao et al., 2016), where pairwise correlations are reduced during active behaviors. However, since somatosensory cortex has been shown to participate in motor control (Mathis et al., 2017; Matyas et al., 2010), the mechanisms generating decorrelation in somatosensory cortex during movement may be unique to this system. Furthermore, the relationship between Vm correlations and functional properties of L2/3 neurons was not investigated in these studies. Here we show that Vm correlations are not strongly dependent on stimulus preference in the visual cortex, indicating that tuning-dependent local connectivity among L2/3 V1 neurons (Ko et al., 2013; Ko et al., 2011) does not strongly contribute to spontaneous membrane potential dynamics during quiet wakefulness.

Taken together, the decreased Vm correlations during active sensing in S1 (Poulet and Petersen, 2008; Zhao et al., 2016) and locomotion in V1 suggest that this effect may be a common feature of activated states in many cortical areas. Indeed, studies in auditory cortex (McGinley et al., 2015a; Schneider et al., 2014), and motor cortex (Schiemann et al., 2015) have all shown similar transitions to asynchronous membrane potential dynamics during movement in single cells. Further work is needed to determine whether common mechanisms underlie these transitions across cortex.

Future directions

We show that activity in visual cortex propagates through L2/3 in highly correlated membrane potential fluctuations. During both spontaneous and visually-evoked activity, cells depolarize in a conserved sequence. These structured patterns of activation are attenuated but not abolished when the animal engages in active behavior. Ordered Vm fluctuations may underlie sequences of spiking activity that have been previously described awake parietal cortex of mice, anesthetized auditory cortex of mice, and anesthetized visual cortex of primate (Euston et al., 2007; Harvey et al., 2012; Jermakowicz et al., 2009; Ji and Wilson, 2007; Luczak et al., 2007). Further work is needed to determine whether cells that fire early or late during these fluctuations represent cell-types participating in distinct stages of visual computation. Ultimately, it will be important to understand how the low and high frequency fluctuations we observe here participate in visual perception by performing multi-cell patch-clamp recordings during behavior.

STAR Methods

CONTACT FOR REAGENT AND RESOURCE SHARING

Further information and requests for resources and reagents should be directed to and will be fulfilled by the Lead Contact, Shaul Hestrin (shestrin@stanford.edu).

EXPERIMENTAL MODEL AND SUBJECT DETAILS

All procedures were approved by the Administrative Panel on Laboratory Animal Care at Stanford University. Male and female C57BL6J mice (JAX Laboratory, stock number 000664) aged 6–12 weeks were used in this study.

METHOD DETAILS

Animals and surgery—To attach headplates, mice were anaesthetized with isoflurane and placed in a stereotaxic frame. Headplates were centered above V1 on the left hemisphere and fixed to the skull with C&BMETABOND® Quick! Cement (Parkell). After surgery, mice were injected with buprenorphine (0.05 mg/kg) and given at least 2 days to recover before the day of recording.

In vivo recording—For whole-cell/whole-cell and whole-cell/LFP recordings, mice were anaesthetized with isoflurane and 2 craniotomies (~100 microns diameter) were made over monocular V1 (2.5–3 mm lateral from lambda). For the LFP-LFP experiments, one reference craniotomy at ~3 mm lateral from lambda was made together with a row of craniotomies ~350 microns anterior and 3 – 1.8 mm lateral to lambda (spaced every ~300 microns). A thin layer of Kwik-Sil (World Precision Instruments) was then applied to the skull until the time of recording. After this procedure, mice were returned to their home cage and given at least two hours to recover before being placed on a spherical treadmill. For whole cell recordings, glass electrodes (4–8 MΩ) were filled with an internal solution composed of the following (in mM): 8 KCl, 115 potassium methyl sulfate (KMS), 9 HEPES, 0.18 EGTA, 4 MgATP, 0.3 NaGTP, 20 sodium phosphocreatine, pH 7.3, 295 mOsm/L. In a subset of recordings, 0.3% biocytin was included in the pipette for *post hoc* cell staining and reconstruction. For LFP recordings, the same electrodes were filled with saline (0.9% sodium chloride). For voltage clamp recordings, KCl and KMS were exchanged for CsCl and CsMS. For the dual WC experiments, standard blind patching techniques were used. Briefly, two pipettes were lowered into the brain under visual guidance with high positive pressure (2.5 PSI). Once in the brain, positive pressure was reduced (0.4 PSI) and both pipettes were advanced simultaneously along a 60-degree axis in short 1–2 μm pulses. If the pipette resistance increased abruptly by 10–20%, positive pressure was released. Only recordings made at a depth of less than 400 μm were included in this study, and depth was confirmed for a subset of recordings by subsequent biocytin staining and cell re-construction. Cell depth measured by distance from the pia in re-constructions was well-matched to the estimates obtained from distance travelled in the micromanipulator. Recordings were performed with a Multiclamp 700B amplifier (Molecular Devices) and digitized by an ITC-18 (InstruTECH). Data acquisition was controlled by custom software written in Igor Pro (Wavemetrics).

Visual Stimulation—Visual stimuli were presented on a gamma-corrected, LED ASUS VK278Q monitor (60 Hz refresh rate, ~75 cd/m^2). Stimuli were generated by custom scripts written in Presentation (Neurobehavioral Systems). The monitor was placed 30 cm from the mouse and subtended ~90 degrees of visual space.

For all of the paired LFP recordings and a subset of the paired WC recordings, the receptive fields were first mapped by presenting a pseudorandom sequence of white squares (20 degrees per side) on a black background. Responses to 5–20 stimuli at each location were acquired and averaged, and a 2D Gaussian was fit to the data to obtain an RF center.

For LFP/LFP and LFP/WC experiments a uniform grey screen was presented for the duration of the experiment after RF mapping. The stimuli for all visual stimulation experiments were full-screen sinusoidal gratings (spatial frequency: 0.05 cycles/degree, velocity: 40^{o}/second, 8 directions) presented for 2 seconds followed by 4–6 seconds of isoluminant gray screen.

Behavioral data acquisition—To monitor speed, we placed an optical mouse on the anterior pole of the spherical treadmill (Fig. 1a). The output from the optical mouse was read with custom software written in Presentation (Neurobehavioral Systems) and converted to an analog signal by a National Instruments NI USB-6008 board.

QUANTIFICATION AND STATISTICAL ANALYSIS

For speed analysis, the raw speed signal was first convolved with a 100 ms boxcar filter. The speed threshold for moving was 5 cm/s. Stationary epochs were defined as periods during which the mean speed was less than 0.5 cm/s. For analysis of spontaneous activity, 2 second epochs were used either (1) between visual stimuli at least ~3 s after the visual stimulus ceased or (2) during prolonged recording with an isoluminant gray screen. Epochs were then binned as stationary or moving based on the speed during these epochs only. For visual stimulation experiments, moving and stationary trials were classified by the mean speed over the visual presentation only.

In Figure 1, LFP signals were band-pass filtered at 1–100 Hz before analysis. Shift predictions in panel G were calculated by calculating CCGs between trial t and t+1.

In Figure 2, raw tuning curves were calculated by averaging the number of spikes elicited by each orientation over the entire duration of the stimulus (~2 s). Double-Gaussian curves were then fit to these data such that the peaks of the Gaussians were separated by 180 degrees. In Supplemental Figure 3, raw tuning curves were calculated by averaging the mean current during the presentation of visual stimulus; double-Gaussian curves were then fit as in Figure 2. OSI was defined from the fit as the (Response(preferred) – Response(opposite))/(Response(preferred) + Response(opposite)).

To compute the temporal offset between current-clamp/current-clamp (CC/CC) and current-clamp/voltage-clamp signals (CC/VC), a cross-correlogram (CCG) was first computed in Matlab for each trial. The lag was then defined as the median offset between the peak of the cross-correlogram from zero. To compute the temporal lag between excitatory and inhibitory conductances, we used a current clamp recording as a reference and computed the CCG for excitation/CC and inhibition/CC separately. Lag between excitation/inhibition was then calculated by calculating the offset between the peaks of the excitation/CC and inhibition/CC CCGs.

In Supplemental Figure 2, depolarized “up” and hyperpolarized “down” phases of fluctuations were identified manually. Points preceding and following a transition were identified in the current clamp recording and used to generate pre- and post-transition mean values. A 25 ms line was then fit centered around the half-amplitude point of the transition. From this transition slope, an onset time was calculated by extrapolating back from the half-amplitude point to the first point that crossed baseline. This onset time was then used to align both the current clamp and voltage clamp recordings.

For spike-triggered analysis, traces were aligned by the time point at which the membrane potential crossed −20 mV and averaged. Threshold was defined as the membrane potential when dV_m/dt reached 3% of its maximum (Azouz and Gray, 2000).

All paired statistical comparisons were performed with the non-parametric Wilcoxon signed-rank test. Non-paired comparisons were performed with the non-parametric Wilcoxon rank-sum test. Coherence and power spectra were calculated using the Chronux package in Matlab. Band pass filtering was computed using the Igor (Wavemetrics) finite impulse response filter (FilterFIR) operation with 4000 coefficients or with a Butterworth filter in Matlab or Python elsewhere.

To detect correlated Vm fluctuations during visual stimulation, the two traces were bandpassed (20–80 Hz) and fluctuations larger than 2.75 mV were used to align and trigger averaging of the two traces (Figure 5D).

DATA AND SOFWARE AVAILABILITY

Analysis was performed using custom software in Matlab which can be made available upon request.

Supplementary Material

Refer to Web version on PubMed Central for supplementary material.

Acknowledgements

This work was supported by the NIH (EY012114 and EY027087 to S.H., Ruth L. Kirschstein Graduate Fellowship and the Medical Scientist Training Program to S.A.), the NSF (Graduate Research Fellowship Program to C.B.), and the Stanford Graduate Fellowship to C.B.

We would also like to thank Alexandar Ortiz for his help with placement of headplates for a subset of these experiments.

References:

Abeles M (1991). Corticonics Neural circuits of the cerebral cortex. (Cambridge, UK: Cambridge UP).

Adesnik H, Bruns W, Taniguchi H, Huang ZJ, and Scanziani M (2012). A neural circuit for spatial summation in visual cortex. Nature 490, 226–231. [PubMed: 23060193]

Averbeck BB, Latham PE, and Pouget A (2006). Neural correlations, population coding and computation. Nat Rev Neurosci 7, 358–366. [PubMed: 16760916]

Azouz R, and Gray CM (2000). Dynamic spike threshold reveals a mechanism for synaptic coincidence detection in cortical neurons in vivo. Proc Natl Acad Sci U S A 97, 8110–8115. [PubMed: 10859358]

Beltramo R, D'Urso G, Dal Maschio M, Farisello P, Bovetti S, Clovis Y, Lassi G, Tucci V, De Pietri Tonelli D, and Fellin T (2013). Layer-specific excitatory circuits differentially control recurrent network dynamics in the neocortex. Nat Neurosci 16, 227–234. [PubMed: 23313909]

Bennett C, Arroyo S, and Hestrin S (2013). Subthreshold mechanisms underlying state-dependent modulation of visual responses. Neuron 80, 350–357. [PubMed: 24139040]

Buzsaki G, and Wang XJ (2012). Mechanisms of gamma oscillations. Annu Rev Neurosci 35, 203–225. [PubMed: 22443509]

Cohen MR, and Kohn A (2011). Measuring and interpreting neuronal correlations. Nat Neurosci 14, 811–819. [PubMed: 21709677]

Cohen-Kashi Malina K, Mohar B, Rappaport AN, and Lampl I (2016). Local and thalamic origins of correlated ongoing and sensory-evoked cortical activities. Nat Commun 7, 12740. [PubMed: 27615520]

Constantinople CM, and Bruno RM (2011). Effects and mechanisms of wakefulness on local cortical networks. Neuron 69, 1061–1068. [PubMed: 21435553]

Cowan RL, and Wilson CJ (1994). Spontaneous firing patterns and axonal projections of single corticostriatal neurons in the rat medial agranular cortex. J Neurophysiol 71, 17–32. [PubMed: 8158226]

Crochet S, and Petersen CC (2006). Correlating whisker behavior with membrane potential in barrel cortex of awake mice. Nat Neurosci 9, 608–610. [PubMed: 16617340]

Doiron B, Litwin-Kumar A, Rosenbaum R, Ocker GK, and Josic K (2016). The mechanics of state-dependent neural correlations. Nat Neurosci 19, 383–393. [PubMed: 26906505]

Dombeck DA, Khabbaz AN, Collman F, Adelman TL, and Tank DW (2007). Imaging large-scale neural activity with cellular resolution in awake, mobile mice. Neuron 56, 43–57. [PubMed: 17920014]

Ecker AS, Berens P, Keliris GA, Bethge M, Logothetis NK, and Tolias AS (2010). Decorrelated neuronal firing in cortical microcircuits. Science 327, 584–587. [PubMed: 20110506]

Einstein MC, Polack PO, Tran DT, and Golshani P (2017). Visually Evoked 3–5 Hz Membrane Potential Oscillations Reduce the Responsiveness of Visual Cortex Neurons in Awake Behaving Mice. J Neurosci 37, 5084–5098. [PubMed: 28432140]

Euston DR, Tatsuno M, and McNaughton BL (2007). Fast-forward playback of recent memory sequences in prefrontal cortex during sleep. Science 318, 1147–1150. [PubMed: 18006749]

Fries P (2005). A mechanism for cognitive dynamics: neuronal communication through neuronal coherence. Trends Cogn Sci 9, 474–480. [PubMed: 16150631]

Gentet LJ, Avermann M, Matyas F, Staiger JF, and Petersen CC (2010). Membrane potential dynamics of GABAergic neurons in the barrel cortex of behaving mice. Neuron 65, 422–435. [PubMed: 20159454]

Gentet LJ, Kremer Y, Taniguchi H, Huang ZJ, Staiger JF, and Petersen CC (2012). Unique functional properties of somatostatin-expressing GABAergic neurons in mouse barrel cortex. Nat Neurosci 15, 607–612. [PubMed: 22366760]

Goard M, and Dan Y (2009). Basal forebrain activation enhances cortical coding of natural scenes. Nat Neurosci 12, 1444–1449. [PubMed: 19801988]

Gregoriou GG, Gotts SJ, Zhou H, and Desimone R (2009). High-frequency, long-range coupling between prefrontal and visual cortex during attention. Science 324, 1207–1210. [PubMed: 19478185]

Haider B, Duque A, Hasenstaub AR, and McCormick DA (2006). Neocortical network activity in vivo is generated through a dynamic balance of excitation and inhibition. J Neurosci 26, 4535–4545. [PubMed: 16641233]

Haider B, Hausser M, and Carandini M (2013). Inhibition dominates sensory responses in the awake cortex. Nature 493, 97–100. [PubMed: 23172139]

Haider B, Schulz DP, Hausser M, and Carandini M (2016). Millisecond Coupling of Local Field Potentials to Synaptic Currents in the Awake Visual Cortex. Neuron 90, 35–42. [PubMed: 27021173]

Harvey CD, Coen P, and Tank DW (2012). Choice-specific sequences in parietal cortex during a virtual-navigation decision task. Nature 484, 62–68. [PubMed: 22419153]

Hofer SB, Ko H, Pichler B, Vogelstein J, Ros H, Zeng H, Lein E, Lesica NA, and Mrsic-Flogel TD (2011). Differential connectivity and response dynamics of excitatory and inhibitory neurons in visual cortex. Nat Neurosci 14, 1045–1052. [PubMed: 21765421]

Jermakowicz WJ, Chen X, Khaytin I, Bonds AB, and Casagrande VA (2009). Relationship between spontaneous and evoked spike-time correlations in primate visual cortex. J Neurophysiol 101, 2279–2289. [PubMed: 19211656]

Ji D, and Wilson MA (2007). Coordinated memory replay in the visual cortex and hippocampus during sleep. Nat Neurosci 10, 100–107. [PubMed: 17173043]

Katzner S, Nauhaus I, Benucci A, Bonin V, Ringach DL, and Carandini M (2009). Local origin of field potentials in visual cortex. Neuron 61, 35–41. [PubMed: 19146811]

Ko H, Cossell L, Baragli C, Antolik J, Clopath C, Hofer SB, and Mrsic-Flogel TD (2013). The emergence of functional microcircuits in visual cortex. Nature 496, 96–100. [PubMed: 23552948]

Ko H, Hofer SB, Pichler B, Buchanan KA, Sjostrom PJ, and Mrsic-Flogel TD (2011). Functional specificity of local synaptic connections in neocortical networks. Nature 473, 87–91. [PubMed: 21478872]

Lampl I, Reichova I, and Ferster D (1999). Synchronous membrane potential fluctuations in neurons of the cat visual cortex. Neuron 22, 361–374. [PubMed: 10069341]

Lemieux M, Chauvette S, and Timofeev I (2015). Neocortical inhibitory activities and long-range afferents contribute to the synchronous onset of silent states of the neocortical slow oscillation. J Neurophysiol 113, 768–779. [PubMed: 25392176]

Luczak A, Bartho P, Marguet SL, Buzsaki G, and Harris KD (2007). Sequential structure of neocortical spontaneous activity in vivo. Proc Natl Acad Sci U S A 104, 347–352. [PubMed: 17185420]

Mathis MW, Mathis A, and Uchida N (2017). Somatosensory Cortex Plays an Essential Role in Forelimb Motor Adaptation in Mice. Neuron 93, 1493–1503 e1496. [PubMed: 28334611]

Matyas F, Sreenivasan V, Marbach F, Wacongne C, Barsy B, Mateo C, Aronoff R, and Petersen CC (2010). Motor control by sensory cortex. Science 330, 1240–1243. [PubMed: 21109671]

McGinley MJ, David SV, and McCormick DA (2015a). Cortical Membrane Potential Signature of Optimal States for Sensory Signal Detection. Neuron 87, 179–192. [PubMed: 26074005]

McGinley MJ, Vinck M, Reimer J, Batista-Brito R, Zagha E, Cadwell CR, Tolias AS, Cardin JA, and McCormick DA (2015b). Waking State: Rapid Variations Modulate Neural and Behavioral Responses. Neuron 87, 1143–1161. [PubMed: 26402600]

Niell CM, and Stryker MP (2010). Modulation of visual responses by behavioral state in mouse visual cortex. Neuron 65, 472–479. [PubMed: 20188652]

Okun M, and Lampl I (2008). Instantaneous correlation of excitation and inhibition during ongoing and sensory-evoked activities. Nat Neurosci 11, 535–537. [PubMed: 18376400]

Okun M, Naim A, and Lampl I (2010). The subthreshold relation between cortical local field potential and neuronal firing unveiled by intracellular recordings in awake rats. J Neurosci 30, 4440–4448. [PubMed: 20335480]

Petersen CC, Hahn TT, Mehta M, Grinvald A, and Sakmann B (2003). Interaction of sensory responses with spontaneous depolarization in layer 2/3 barrel cortex. Proc Natl Acad Sci U S A 100, 13638–13643. [PubMed: 14595013]

Polack PO, Friedman J, and Golshani P (2013). Cellular mechanisms of brain state-dependent gain modulation in visual cortex. Nat Neurosci 16, 1331–1339. [PubMed: 23872595]

Poulet JF, and Petersen CC (2008). Internal brain state regulates membrane potential synchrony in barrel cortex of behaving mice. Nature 454, 881–885. [PubMed: 18633351]

Reimer J, Froudarakis E, Cadwell CR, Yatsenko D, Denfield GH, and Tolias AS (2014). Pupil fluctuations track fast switching of cortical states during quiet wakefulness. Neuron 84, 355–362. [PubMed: 25374359]

Reimer J, McGinley MJ, Liu Y, Rodenkirch C, Wang Q, McCormick DA, and Tolias AS (2016). Pupil fluctuations track rapid changes in adrenergic and cholinergic activity in cortex. Nat Commun 7, 13289. [PubMed: 27824036]

Rothschild G, Eban E, and Frank LM (2017). A cortical-hippocampal-cortical loop of information processing during memory consolidation. Nat Neurosci 20, 251–259. [PubMed: 27941790]

Salkoff DB, Zagha E, Yuzgec O, and McCormick DA (2015). Synaptic Mechanisms of Tight Spike Synchrony at Gamma Frequency in Cerebral Cortex. J Neurosci 35, 10236–10251. [PubMed: 26180200]

Schiemann J, Puggioni P, Dacre J, Pelko M, Domanski A, van Rossum MC, and Duguid I (2015). Cellular mechanisms underlying behavioral state-dependent bidirectional modulation of motor cortex output. Cell Rep 11, 1319–1330. [PubMed: 25981037]

Schneider DM, Nelson A, and Mooney R (2014). A synaptic and circuit basis for corollary discharge in the auditory cortex. Nature 513, 189–194. [PubMed: 25162524]

Sheroziya M, and Timofeev I (2014). Global intracellular slow-wave dynamics of the thalamocortical system. J Neurosci 34, 8875–8893. [PubMed: 24966387]

Siapas AG, and Wilson MA (1998). Coordinated interactions between hippocampal ripples and cortical spindles during slow-wave sleep. Neuron 21, 1123–1128. [PubMed: 9856467]

Sirota A, Csicsvari J, Buhl D, and Buzsaki G (2003). Communication between neocortex and hippocampus during sleep in rodents. Proc Natl Acad Sci U S A 100, 2065–2069. [PubMed: 12576550]

Steriade M, Nunez A, and Amzica F (1993). A novel slow (< 1 Hz) oscillation of neocortical neurons in vivo: depolarizing and hyperpolarizing components. J Neurosci 13, 3252–3265. [PubMed: 8340806]

Steriade M, Timofeev I, and Grenier F (2001). Natural waking and sleep states: a view from inside neocortical neurons. J Neurophysiol 85, 1969–1985. [PubMed: 11353014]

Tan AY, Chen Y, Scholl B, Seidemann E, and Priebe NJ (2014). Sensory stimulation shifts visual cortex from synchronous to asynchronous states. Nature 509, 226–229. [PubMed: 24695217]

Tiesinga P, and Sejnowski TJ (2009). Cortical enlightenment: are attentional gamma oscillations driven by ING or PING? Neuron 63, 727–732. [PubMed: 19778503]

Timofeev I, Grenier F, Bazhenov M, Sejnowski TJ, and Steriade M (2000). Origin of slow cortical oscillations in deafferented cortical slabs. Cereb Cortex 10, 1185–1199. [PubMed: 11073868]

Timofeev I, Grenier F, and Steriade M (2001). Disfacilitation and active inhibition in the neocortex during the natural sleep-wake cycle: an intracellular study. Proc Natl Acad Sci U S A 98, 1924–1929. [PubMed: 11172052]

Veit J, Hakim R, Jadi MP, Sejnowski TJ, and Adesnik H (2017). Cortical gamma band synchronization through somatostatin interneurons. Nat Neurosci.

Volgushev M, Chauvette S, Mukovski M, and Timofeev I (2006). Precise long-range synchronization of activity and silence in neocortical neurons during slow-wave oscillations [corrected]. J Neurosci 26, 5665–5672. [PubMed: 16723523]

Wang Q, and Burkhalter A (2007). Area map of mouse visual cortex. J Comp Neurol 502, 339–357. [PubMed: 17366604]

Wilson CJ, and Groves PM (1981). Spontaneous firing patterns of identified spiny neurons in that rat neostriatum. Brain Res 220, 67–80. [PubMed: 6168334]

Yu J, and Ferster D (2010). Membrane potential synchrony in primary visual cortex during sensory stimulation. Neuron 68, 1187–1201. [PubMed: 21172618]

Zagha E, Casale AE, Sachdev RN, McGinley MJ, and McCormick DA (2013). Motor cortex feedback influences sensory processing by modulating network state. Neuron 79, 567–578. [PubMed: 23850595]

Zhao WJ, Kremkow J, and Poulet JF (2016). Translaminar Cortical Membrane Potential Synchrony in Behaving Mice. Cell Rep 15, 2387–2399. [PubMed: 27264185]

Highlights

- Vm correlations in V1 depend on behavioral state but not tuning similarity
- Visual stimulation reduces low-frequency and generates high-frequency Vm coherence
- Inhibition lags excitation by ~5 ms during correlated Vm fluctuations
- Neurons activate in a conserved sequence across stimulus and behavioral states

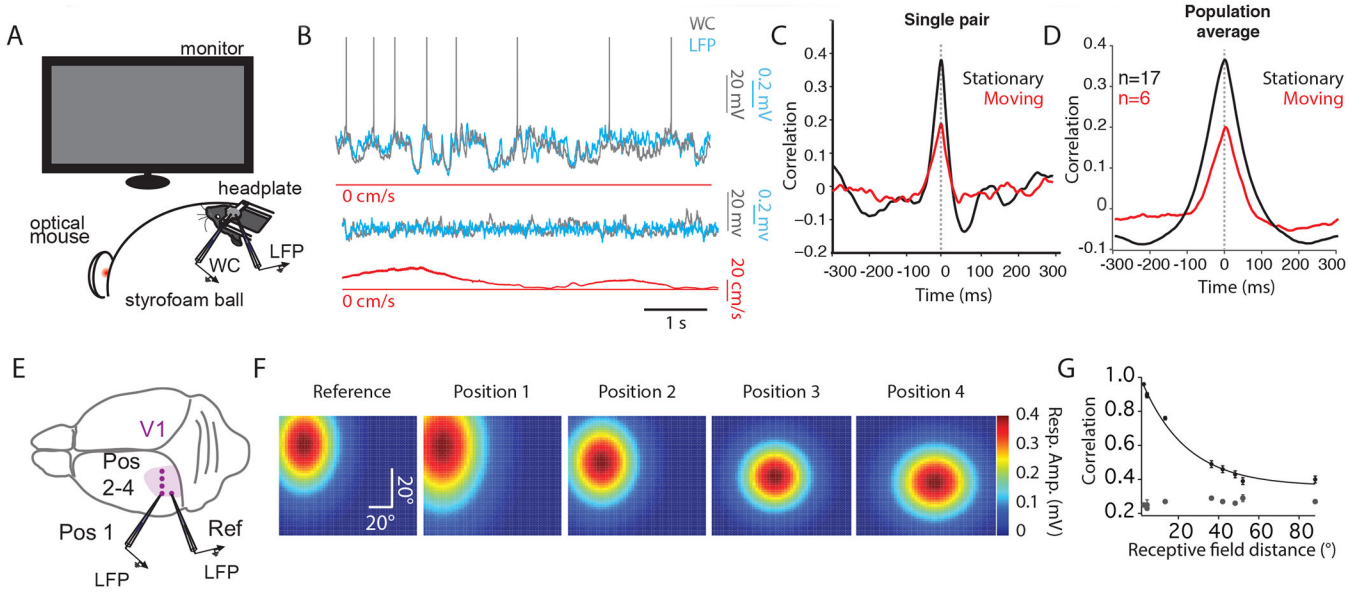

Figure 1: The spatial extent of correlated activity in the visual cortex of awake, behaving mice.

(A) Schematic illustrating experimental set-up.

(B) Simultaneous WC (gray), and LFP (cyan), and speed (red) recordings during stationary (upper) and moving (lower) epochs. LFP is inverted for display purposes.

(C) Cross-correlogram for the pair in (B) for stationary (black) and moving (red) epochs. Dotted line represents zero lag for (C) and (D).

(D) Averaged cross-correlogram for 17 WC/LFP pairs during stationary epochs (black). In 6 of these pairs, moving epochs were also measured (red).

(E) Cartoon illustrating the pattern of craniotomies in V1 used for LFP-LFP experiments.

(F) 2D Gaussian fits to receptive field maps for LFP position marked in (E). Color legend is depicted on the right.

(G) Relationship between Pearson's r and receptive field distance in degrees. Gray dots represent shift-predicted correlation values.

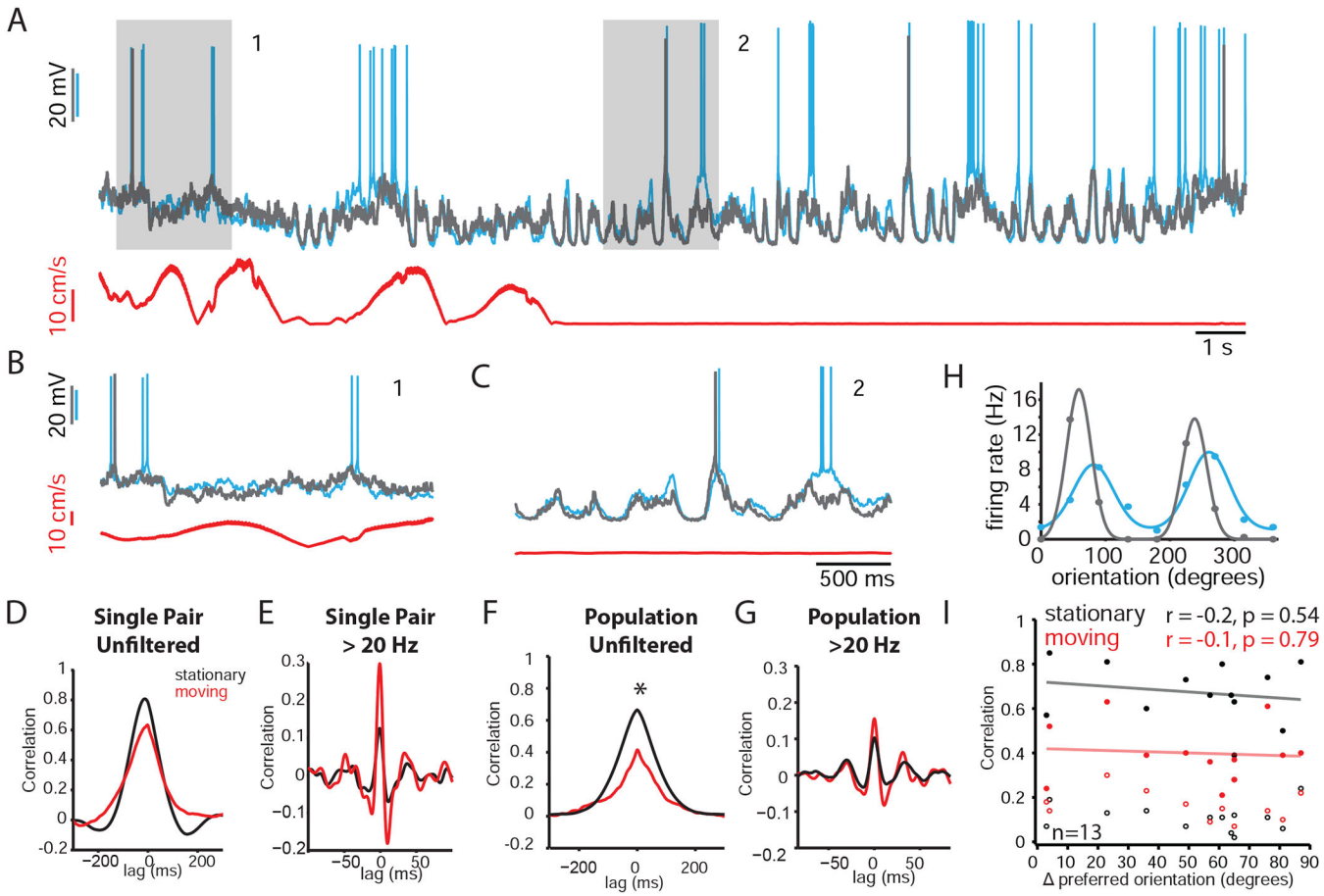

Figure 2: Spontaneous membrane potential correlations are independent of stimulus preference.

(A) Two simultaneous WC current clamp recordings (cyan and gray), together with a speed trace (red). Gray boxes highlight a moving (1) and stationary (2) epoch expanded in (B) and (C), respectively.

(B) Expanded timescale for moving epoch (1) highlighted in gray in (A).

(C) Expanded timescale for stationary epoch (2) highlighted in gray in (A).

(D) Cross-correlogram for pair shown in A-C. Black and red traces represent analysis for stationary and moving epochs, respectively. The same color scheme is used in E, F, G, and I.

(E) Cross-correlogram for pair in (A) after high-pass filtering the signals at >20 Hz.

(F) Population average (n=13). Black bar represents region of significant statistical difference

(G) Population average (n=13) for analysis in (E).

(H) Tuning curves for cells shown in (A).

(I) Pearson's *r* for unfiltered (solid symbols) and filtered > 20 Hz (open symbols) as a function of tuning disparity during stationary (black) and moving (red) epochs. Neither moving nor stationary correlation exhibited a significant correlation with tuning disparity (r = −0.2, p = 0.54 for stationary unfiltered; r = −0.1, p = 0.79 for moving unfiltered; r = −0.08, p = 0.79 for stationary filtered; r = −0.23, p = 0.48 for moving filtered; n = 13).

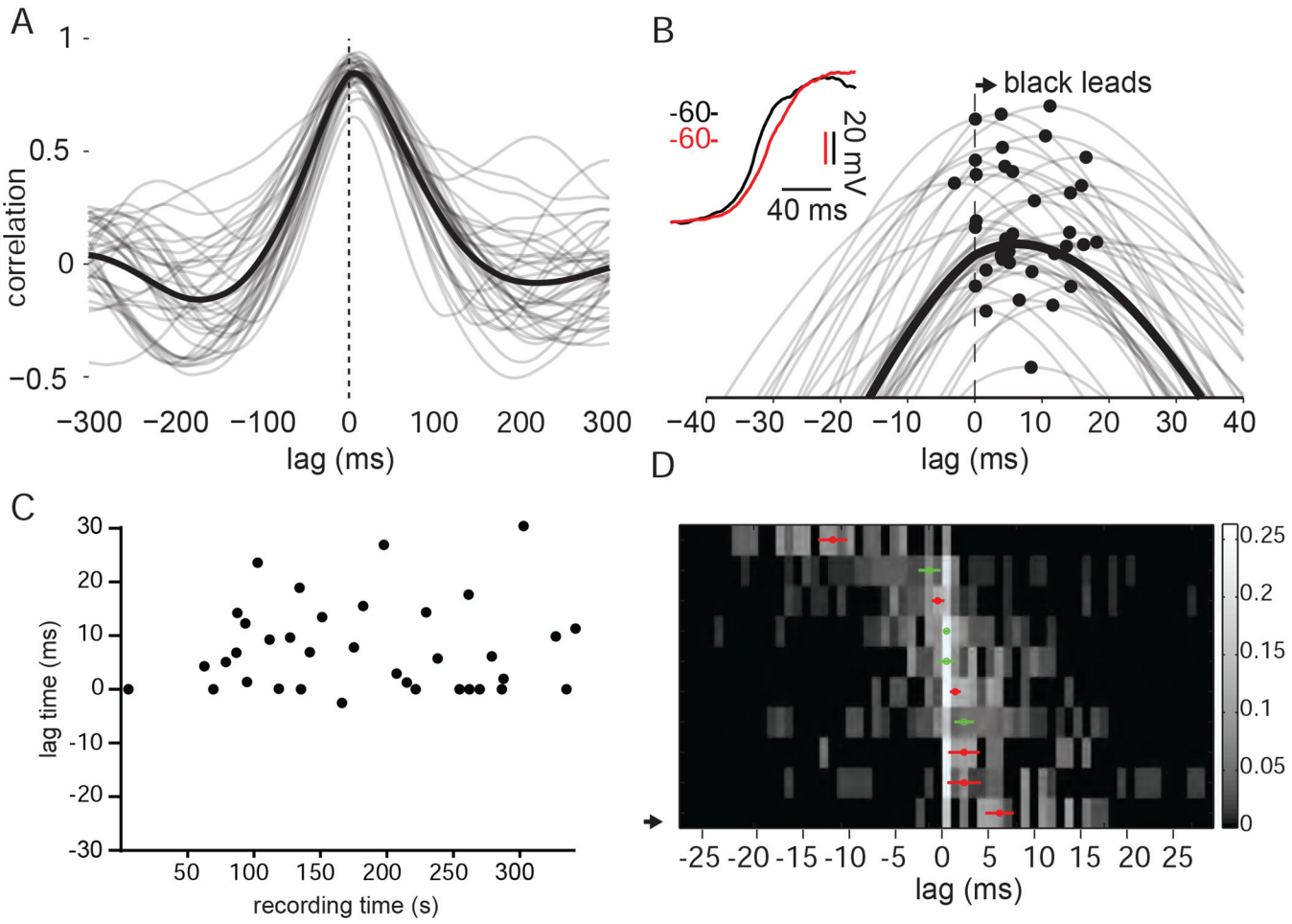

Figure 3: The sign of Vm lag between pairs of L2/3 neurons is preserved over time

(A) Vm CCG for a pair of L2/3 neurons computed with 2 s segments during epochs of quiet wakefulness. Single trial CCGs are displayed in gray; mean CCG is displayed in black.

(B) Expanded timescale highlighting CCG offset from zero in (A). Peak of the CCGs are marked with filled black circles.

(C) CCG offsets plotted over recording time for pair in (A) and (B).

(D) Heat map representing CCG offsets for population of 10 pairs. Each row is a probability distribution of CCG offsets for one pair. A small number of trials had offsets larger than 30 ms and are not displayed. The median CCG offset for each pair is marked by a red circle for those distributions significantly different from zero and green open circles for those that are not. Error bars reflect the standard error of the mean. (solid, significantly different from zero; open, not significantly different from zero).

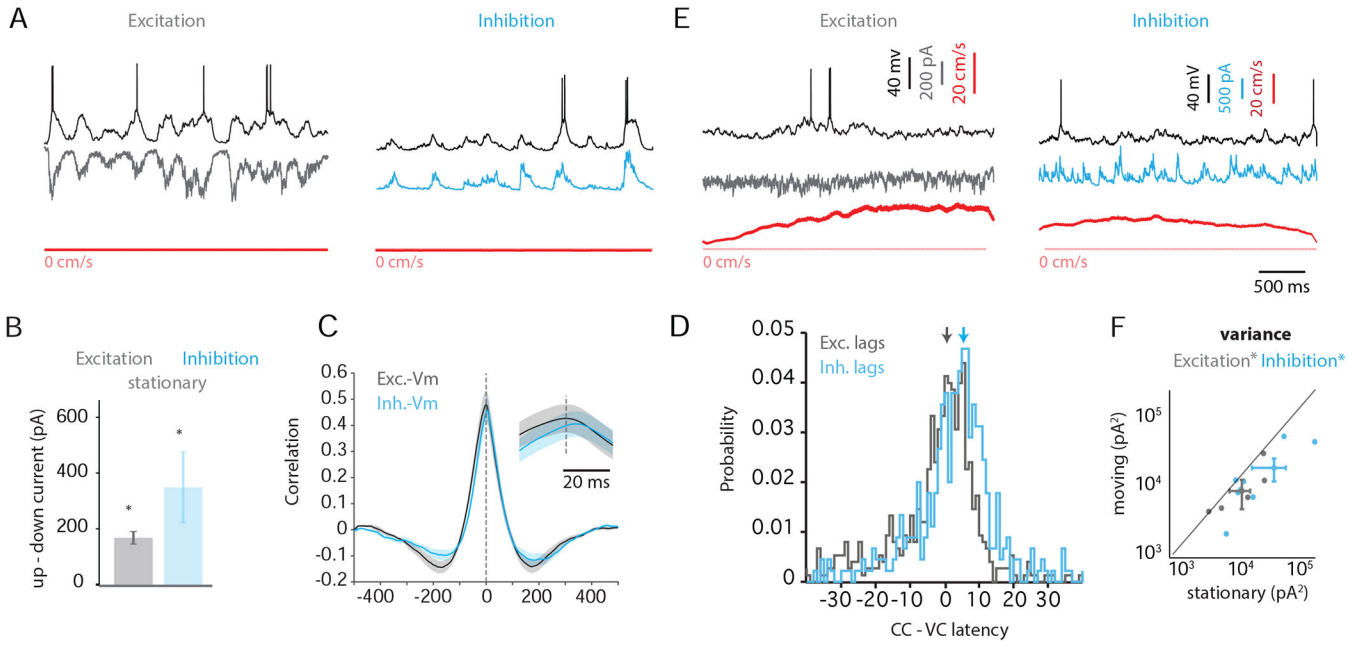

Figure 4: Role of excitation and inhibition in generating Vm correlations during quiet wakefulness and locomotion.

(A) Simultaneous current clamp recording (black), voltage clamp recording, and speed trace (red) during quiet wakefulness. Voltage-clamped cell is being held at the reversal potential for inhibition (left, gray) or excitation (right, cyan).

(B) Difference in current between the “up” and “down” phases of fluctuations during quiet wakefulness for excitation (gray) and inhibition (cyan).

(C) Mean CCGs for excitation/Vm (gray) and inhibition/Vm (cyan). Inset, expanded timescale.

(D) Histogram of median lags from excitation/Vm CCGs (gray) and inhibition/Vm CCGs (cyan) across all pairs (n = 7). Arrows denote the peak in the histograms. The x-axis is time relative to the peak of the excitation/Vm histogram.

(E) As in (A) for moving epochs. (F) Variance in excitatory (gray) and inhibitory (cyan) currents is plotted for moving vs. stationary epochs. *, $p < 0.05$.

See also Figure S1.

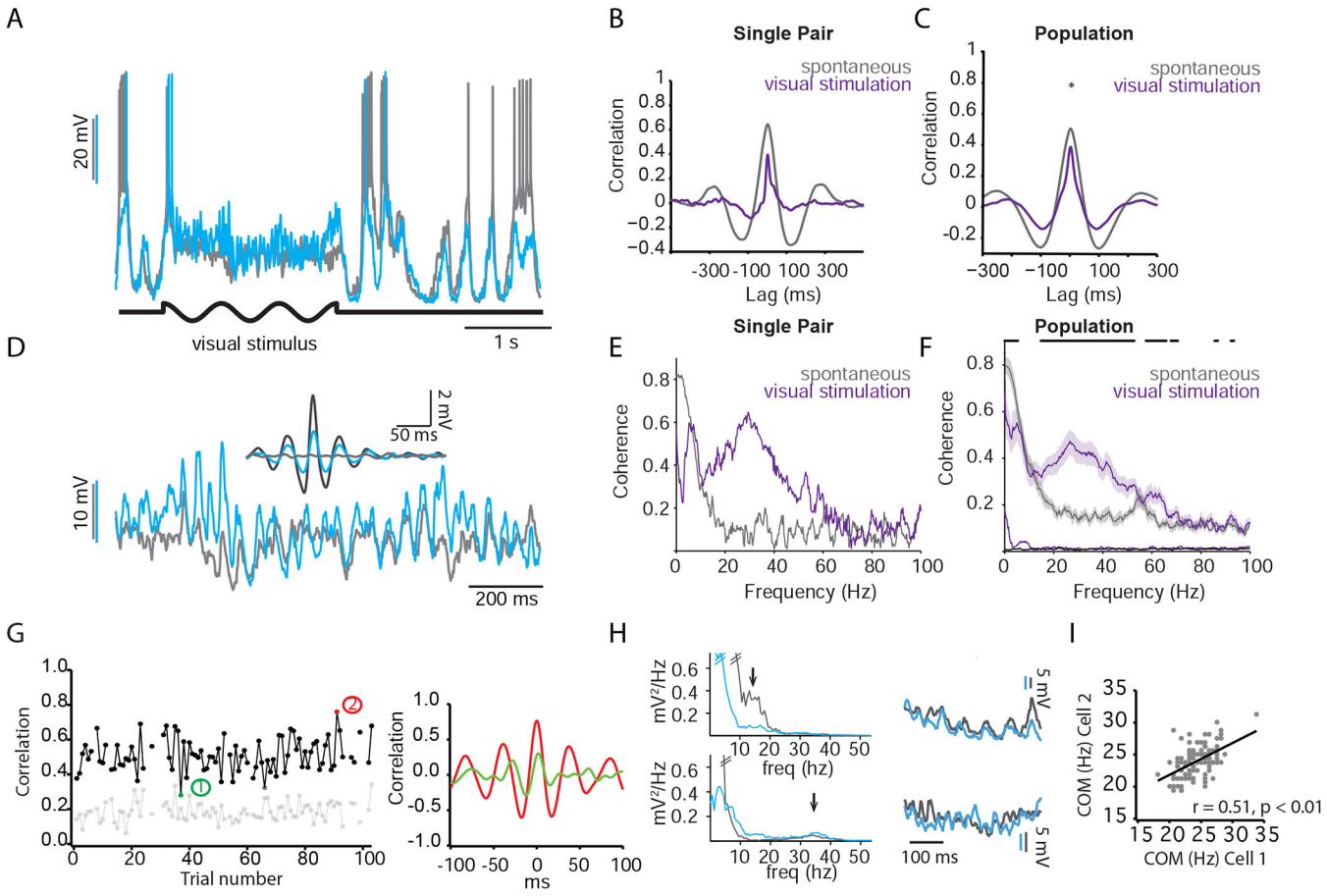

Figure 5: Visual stimulation generates high-frequency correlations and preserves sign of Vm lag between pairs.

(A) Dual current clamp recordings from L2/3 pyramidal neurons. Black trace denotes epoch of visual stimulation.

(B) Cross-correlogram between pair of neurons during spontaneous (gray trace) and visual stimulation (purple trace) epochs for the pair in (A)

(C) Same as (B) for population, n=10. * denotes significance for statistical comparison at zero lag.

(D) expanded timescale taken from epoch of visual stimulation in (A). Inset, fluctuation-triggered (> 2.75 mV) averaging of band-passed (15–50 Hz) traces.

(E) Coherence plotted as a function of frequency for spontaneous and visual stimulation epochs in (A).

(F) Same as (E) for population.

(G) Vm correlations during visual stimulation are plotted across trials. Gaps represent moving trials, which were omitted from the plot. Light gray trace represents the shuffled correlation obtained by computing the cross correlogram between trial n from cell 1 and trial n+1 from cell 2. Right, example cross correlograms from trials (1) and (2) highlighted in plot on left.

(H) Power spectra for two example trials are displayed (top and bottom). Arrowheads denote relative peaks in these spectra seen in these two trials, the first at ~15 Hz and the second at ~35 Hz. Right, example waveforms from the trials used to generate spectra on left.
(I) The frequency center of mass (COM) for power in the beta frequency band (15–40 Hz) for cell 2 plotted against the COM for cell 1.
See also Figure S2.

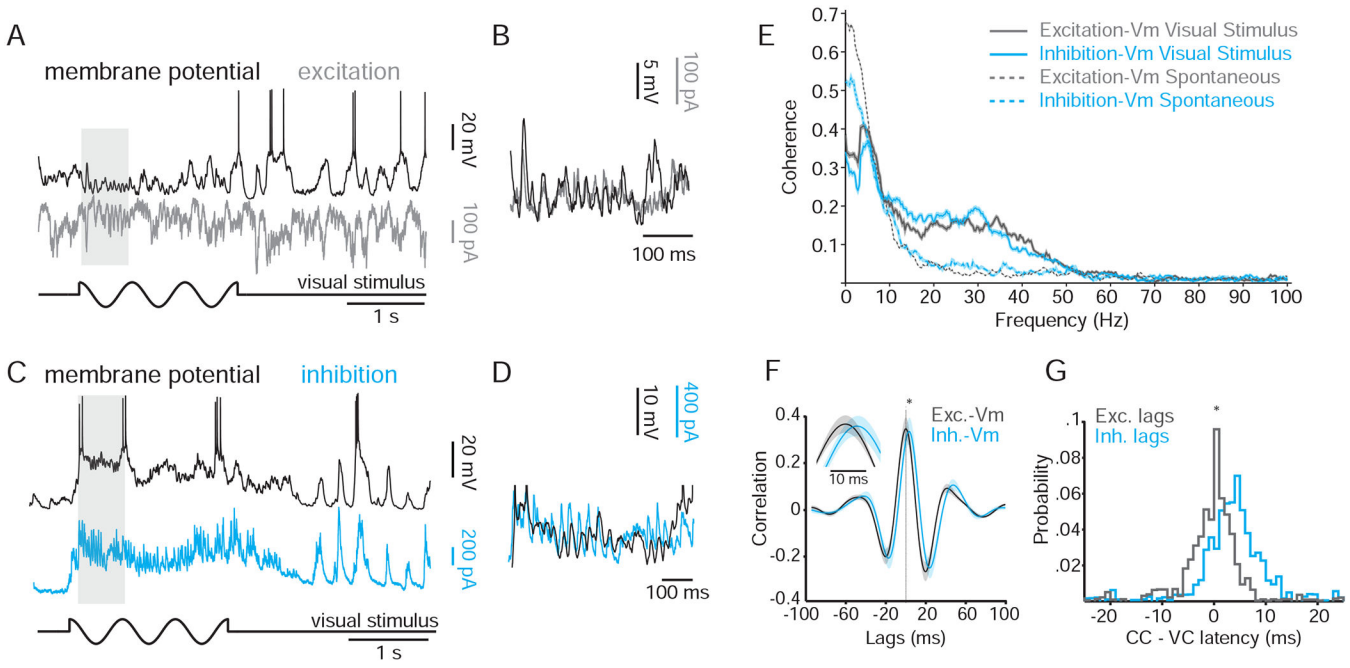

Figure 6: High frequency Vm fluctuations during visual stimulus are driven by excitation and inhibition

(A) Simultaneous current-clamp (black) and voltage-clamp (held at inhibitory reversal potential; gray) recordings during quiet wakefulness. Black trace below recordings denotes the timing of the visual stimulation.

(B) Inset for epoch highlighted by the gray box in (A).

(C) Same as (A), except cyan trace is a voltage clamp recording held at the excitatory reversal potential.

(D) Inset for epoch highlighted by the gray box in (C).

(E) Coherence between current-clamp and voltage-clamp recordings during spontaneous activity (dotted lines) and visual stimulation (solid lines).

(F) Averaged cross correlogram of excitation vs. Vm and inhibition vs. Vm for all pairs (n = 7). Inset, expanded timescale showing temporal offset between the two cross-correlograms.

(G) Probability distribution of CCG offsets for excitation vs. Vm (gray) and inhibition vs. Vm (cyan), centered around median excitation vs. Vm offset.

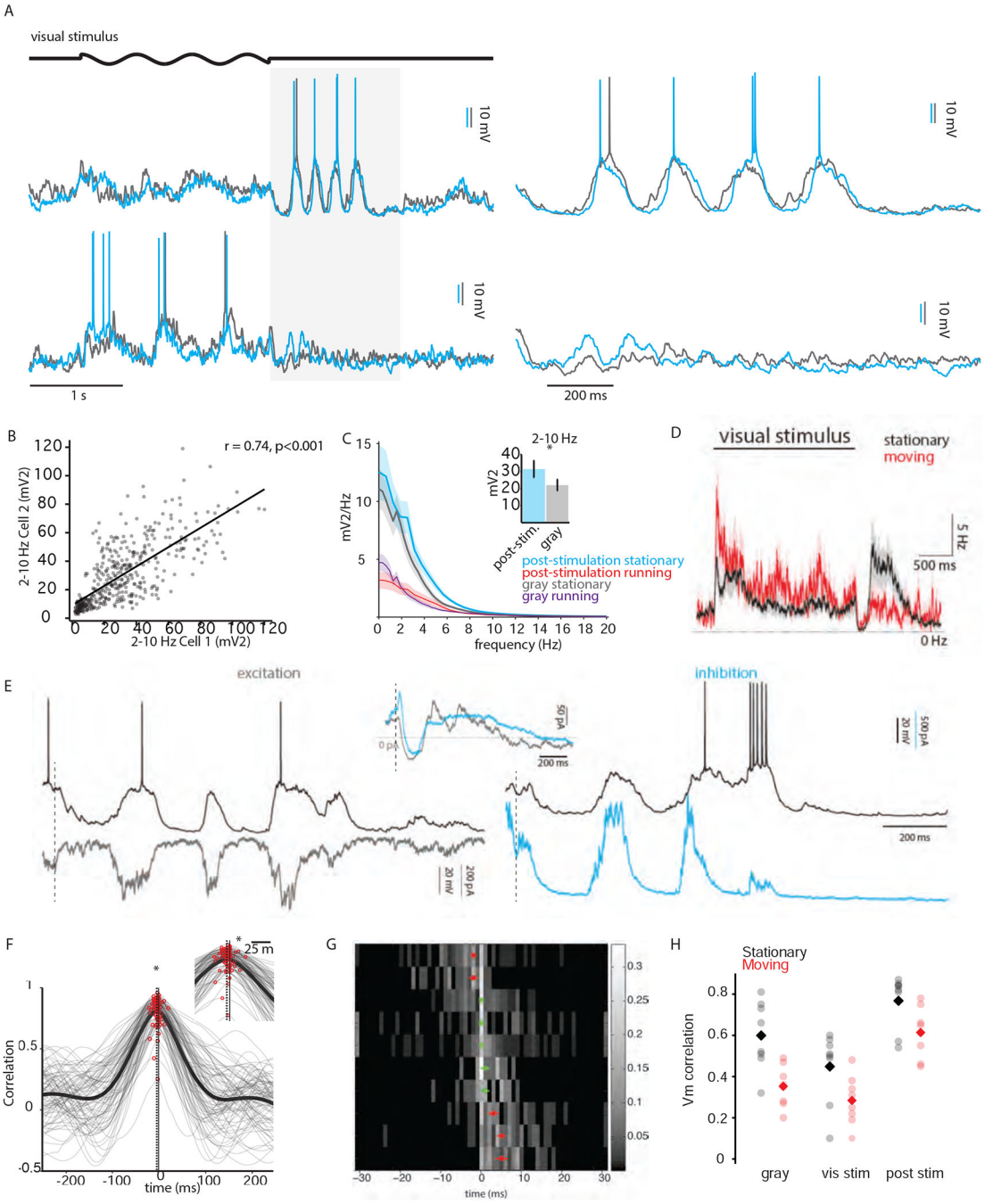

Figure 7: Low-frequency, high-amplitude correlated activity following visual stimulation preserves temporal lag between pairs.

(A) Two example experimental trials during the stationary (above) and moving (below) behavioral states. An epoch just following the visual stimulus (light gray box) is expanded to the right.

(B) Power in the 2–10 Hz band was calculated for each simultaneously recorded pair of cells under current clamp conditions and plotted against each other for the stationary epochs.

(C) Power spectra comparing post-stimulation and no-stimulation (gray) epochs during the stationary and moving behavioral states for all cells. Inset, power in the 2–10 Hz band for the stationary state during the post-stimulation and gray epochs. *, $p < 0.05$.
(D) The PSTH averaged across all cells (n=20) for the stationary (black) and moving (red) states. The standard error of the mean is depicted by the transparent envelopes around the solid traces.
(E) Simultaneous current clamp (black traces) and voltage clamp recordings (gray and cyan traces) during the post-stimulation epoch. Left, voltage clamp recording held at reversal potential for inhibition (gray). Right, voltage clamp recording held at reversal potential for excitation (cyan). Inset, grand average of excitatory and inhibitory waveforms across all cells (n = 8) during the post-stimulation epoch. The excitatory waveform has been inverted for clarity. Vertical dotted lines mark the end of the visual stimulus.
(F) Trial-to-trial Vm CCGs for an example pair during the post-stimulation epoch are shown in gray together with the mean CCG shown in black. The vertical solid line represents zero lag while the vertical dotted line represents the median lag of the trial-to-trial CCGs.
(G) As in previous figures, heat map representing the Vm CCG offsets for 10 pairs during the post-stimulation epoch. Red dots represent the median CCG offset for each row for distribution significantly offset from zero; open green symbols re not significantly offset from zero. Error bars represent the standard error of the mean.
(H) Mean Vm correlations for spontaneous, visually-evoked and post-stimulus activity during stationary (black) and running (red) epochs. Circles represent data from individual pairs. Diamonds are population means.
See also Figure S3.

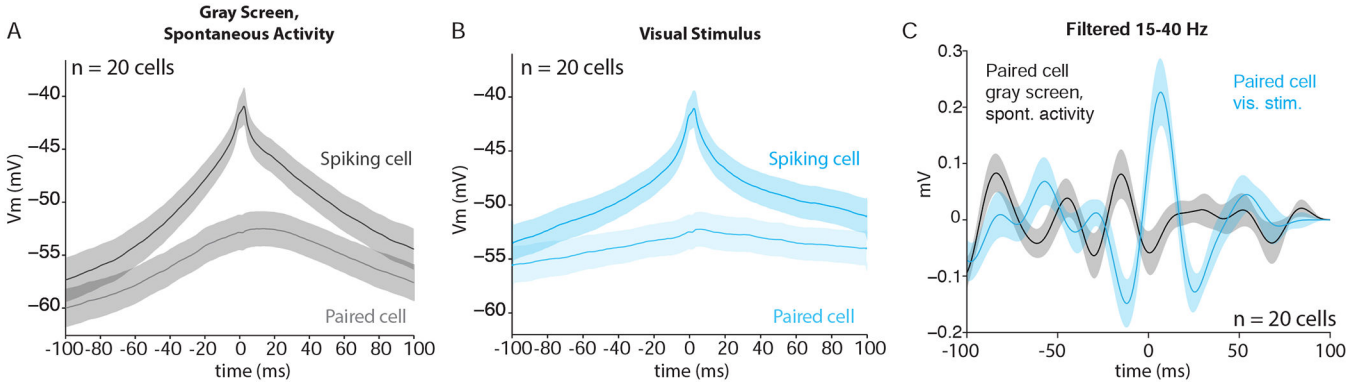

Figure 8: Inputs leading to spikes are sharper and more coordinated during visually-evoked activity

(A) Spike-triggered average (STA) of membrane potential for the spiking cell (dark gray) and the paired cell (light gray) during spontaneous activity (n=20). Traces are means across all pairs. Shaded regions represent standard error. Note that the spike in the top trace is truncated for display.

(B) Same as (A) but for visually-evoked activity (n=20).

(C) Band-pass filtered STA (15–40 Hz) of membrane potential for paired cell during visually-evoked (blue) and spontaneous (gray) activity (n=20).